# Role of kinesin-1–based microtubule sliding in *Drosophila* nervous system development

Michael Winding[a], Michael T. Kelliher[b,c], Wen Lu[a], Jill Wildonger[b], and Vladimir I. Gelfand[a,1]

[a]Department of Cell and Molecular Biology, Feinberg School of Medicine, Northwestern University, Chicago, IL 60611; [b]Department of Biochemistry, University of Wisconsin-Madison, Madison, WI 53706; and [c]Integrated Program in Biochemistry, University of Wisconsin-Madison, Madison, WI 53706

Edited by J. Richard McIntosh, University of Colorado, Boulder, CO, and approved June 17, 2016 (received for review November 13, 2015)

**The plus-end microtubule (MT) motor kinesin-1 is essential for normal development, with key roles in the nervous system. Kinesin-1 drives axonal transport of membrane cargoes to fulfill the metabolic needs of neurons and maintain synapses. We have previously demonstrated that kinesin-1, in addition to its well-established role in organelle transport, can drive MT–MT sliding by transporting "cargo" MTs along "track" MTs, resulting in dramatic cell shape changes. The mechanism and physiological relevance of this MT sliding are unclear. In addition to its motor domain, kinesin-1 contains a second MT-binding site, located at the C terminus of the heavy chain. Here, we mutated this C-terminal MT-binding site such that the ability of kinesin-1 to slide MTs is significantly compromised, whereas cargo transport is unaffected. We introduced this mutation into the genomic locus of kinesin-1 heavy chain (KHC), generating the $Khc^{mutA}$ allele. $Khc^{mutA}$ neurons displayed significant MT sliding defects while maintaining normal transport of many cargoes. Using this mutant, we demonstrated that MT sliding is required for axon and dendrite outgrowth in vivo. Consistent with these results, $Khc^{mutA}$ flies displayed severe locomotion and viability defects. To test the role of MT sliding further, we engineered a chimeric motor that actively slides MTs but cannot transport organelles. Activation of MT sliding in $Khc^{mutA}$ neurons using this chimeric motor rescued axon outgrowth in cultured neurons and in vivo, firmly establishing the role of sliding in axon outgrowth. These results demonstrate that MT sliding by kinesin-1 is an essential biological phenomenon required for neuronal morphogenesis and normal nervous system development.**

kinesin-1 | microtubules | *Drosophila* | axon outgrowth | dendrite outgrowth

Neurons are the basic unit of the nervous system, forming vast networks throughout the body that communicate using receptor-ligand machinery located in long cellular projections called axons and dendrites. Learning how these processes form is key to understanding the early development and pathology of the nervous system. Microtubules (MTs) and actin microfilaments have been implicated in neurite outgrowth, with many studies focusing on the growth cone at the tip of the axon. Previous models suggest that the driving forces for neurite outgrowth are MT polymerization and the treadmilling of F-actin (1, 2). However, other studies demonstrate that F-actin is dispensable to outgrowth and neurites extend even in the absence of F-actin (3–5).

Our group has found that the motor protein kinesin-1 can rearrange the MT network by sliding MTs against each other (6). We have shown that kinesin-1 is required for MT sliding in cultured neurons and kinesin-1 depletion inhibits both neurite outgrowth and regeneration (7, 8). Additionally, we have observed MT sliding in axons as well as MTs pushing on the axon tip (9). Recent studies from other groups have also implicated MT translocation in axon extension and dendritic organization (10–12). Based on these studies, we hypothesize that kinesin-1 drives neurite extension by sliding MTs against the plasma membrane. Consistent with this model, kinesin-1 depletion in vivo has severe phenotypes in the nervous system. Knockout of kinesin-1 in *Drosophila* results in locomotion defects and eventual death during the larval stages due to nervous system dysfunction (13, 14). However, because kinesin-1 engages in both MT sliding and organelle transport, it is hard to determine which phenotypes are caused by a deficiency in MT sliding. To test the role of MT sliding in neurite outgrowth directly, we set out to create a sliding-deficient kinesin-1 mutant that can dissociate the roles of kinesin-1 in sliding and organelle transport.

A previous study demonstrated that human kinesin-1 heavy chain (KHC) contains an additional MT-binding site besides the motor domain (15). Biochemical studies mapped this site to positively charged residues at the extreme C terminus of the heavy chain (16–18). Based on these studies, we hypothesized that KHC engages in MT sliding by binding one MT with its C-terminal MT-binding site while walking along a second MT using its motor domain. Here, we demonstrate that this C-terminal MT-binding site is required for MT sliding and introduce a sliding-deficient KHC mutant, which allowed us to determine the physiological role of MT sliding. We introduced this sliding-deficient mutant into the endogenous *Khc* locus and demonstrated that MT sliding is required for *Drosophila* nervous system development. We also engineered a chimeric motor protein containing the motor domain of kinesin-3 fused to the extreme C terminus of kinesin-1, including its MT-binding site. This motor is able to slide MTs, but it cannot transport organelles. Expressing this chimeric motor in our MT sliding-deficient KHC flies rescued axon outgrowth phenotypes both in cultured neurons and in vivo, further demonstrating the importance of sliding in neurodevelopment.

## Results

**Kinesin-1 Slides MTs Using Its C-Terminal–Binding Site.** We have previously shown that kinesin-1 slides cytoplasmic MTs in *Drosophila* and mammalian cells (6, 7). We hypothesized that kinesin-1 engages in MT sliding by binding one MT using the MT-binding

### Significance

We previously demonstrated that the microtubule (MT) motor protein kinesin-1 slides and transports MTs themselves in addition to its established role in organelle transport. However, the physiological importance of MT sliding has not been determined. Here, we identified the mechanism of kinesin-1–based MT sliding and generated a sliding-deficient *Drosophila* mutant. Additionally, we generated a chimeric motor that actively slides MTs but cannot transport organelles. Using these tools, we demonstrated that MT sliding is an essential biological process, with key roles in both axon and dendrite outgrowth. Because the C-terminal MT-binding site of kinesin-1, which is essential for sliding, is highly conserved in vertebrates and invertebrates, we postulate that MT sliding is important for nervous system development in many organisms.

Author contributions: M.W., W.L., J.W., and V.I.G. designed research; M.W. and W.L. performed research; M.T.K. and J.W. contributed new reagents/analytic tools; M.W., W.L., and V.I.G. analyzed data; and M.W., W.L., and V.I.G. wrote the paper.

The authors declare no conflict of interest.

This article is a PNAS Direct Submission.

[1]To whom correspondence should be addressed. Email: vgelfand@northwestern.edu.

This article contains supporting information online at www.pnas.org/lookup/suppl/doi:10.1073/pnas.1522416113/-/DCSupplemental.

site at the extreme C terminus of the heavy chain (15–17) while the motor domain walks on another MT. To test this hypothesis, we mutated the C-terminal MT-binding site of KHC based on a previous study on human kinesin-1 (17). We mutated four residues (R914A, K915A, R916A, and Q918A) in the C-terminal MT-binding site, generating KHC$^{mutA}$ (Fig. 1*A*). To test whether these alanine mutations reduced MT binding, we purified short kinesin-1 fragments (amino acids 844–959) with or without alanine mutations (K959 and K959$^{mutA}$, respectively) from *Escherichia coli*. We found that K959 bound MTs with a submicromolar affinity [$K_d = 0.45 \pm 0.08$ μM (average ± SD)], whereas K959$^{mutA}$ bound with a significantly weaker affinity ($K_d = 1.37 \pm 0.16$ μM) (Fig. 1*B*). To test whether KHC$^{mutA}$ affected MT affinity in cells, we generated *Drosophila* S2 cell lines expressing GFP-tagged wild-type KHC or KHC$^{mutA}$ tails (amino acids 345–975). As described previously (15), GFP-KHC tail decorated MTs in S2 cells and remained bound to MTs after extraction of soluble proteins with detergent (Fig. 1*C*). Conversely, significantly more GFP-KHC$^{mutA}$ tail was extracted from the cells after detergent treatment, demonstrating that KHC$^{mutA}$ has diminished MT binding in cells (Fig. 1 *C* and *D*).

To test whether the C-terminal MT-binding site of KHC is necessary for MT sliding, we assayed MT sliding using α-tubulin tagged with a tandem dimer of the photoconvertible probe EOS (tdEOS-tubulin) (9, 19), which changes emission spectra from green to red upon exposure to UV light (20). To quantify MT sliding, we expressed tdEOS-tubulin in *Drosophila* S2 cells, photoconverted a small subset of MTs from green to red, and imaged converted MTs in the red channel. To test whether KHC$^{mutA}$ can slide MTs, we depleted endogenous KHC with dsRNA targeting its 3′-UTR and cotransfected KHC$^{mutA}$ and tdEOS-tubulin. KHC$^{mutA}$ was tagged with blue fluorescent protein (BFP) so that we could assess expression (21). BFP-tagged wild-type KHC was used as a control for these experiments. We found that KHC$^{mutA}$ displayed greatly reduced MT sliding compared with control (Fig. 2 *B* and *C* and Movie S1). To test further if KHC$^{mutA}$ is sliding-deficient, we assayed a MT sliding-based activity. Kinesin-1–dependent sliding has been shown to drive the formation of cellular processes in S2 cells after F-actin depolymerization (6, 22). We quantified the length of processes generated by either KHC or KHC$^{mutA}$. In agreement with the MT sliding data, KHC$^{mutA}$ generated significantly shorter processes compared with KHC

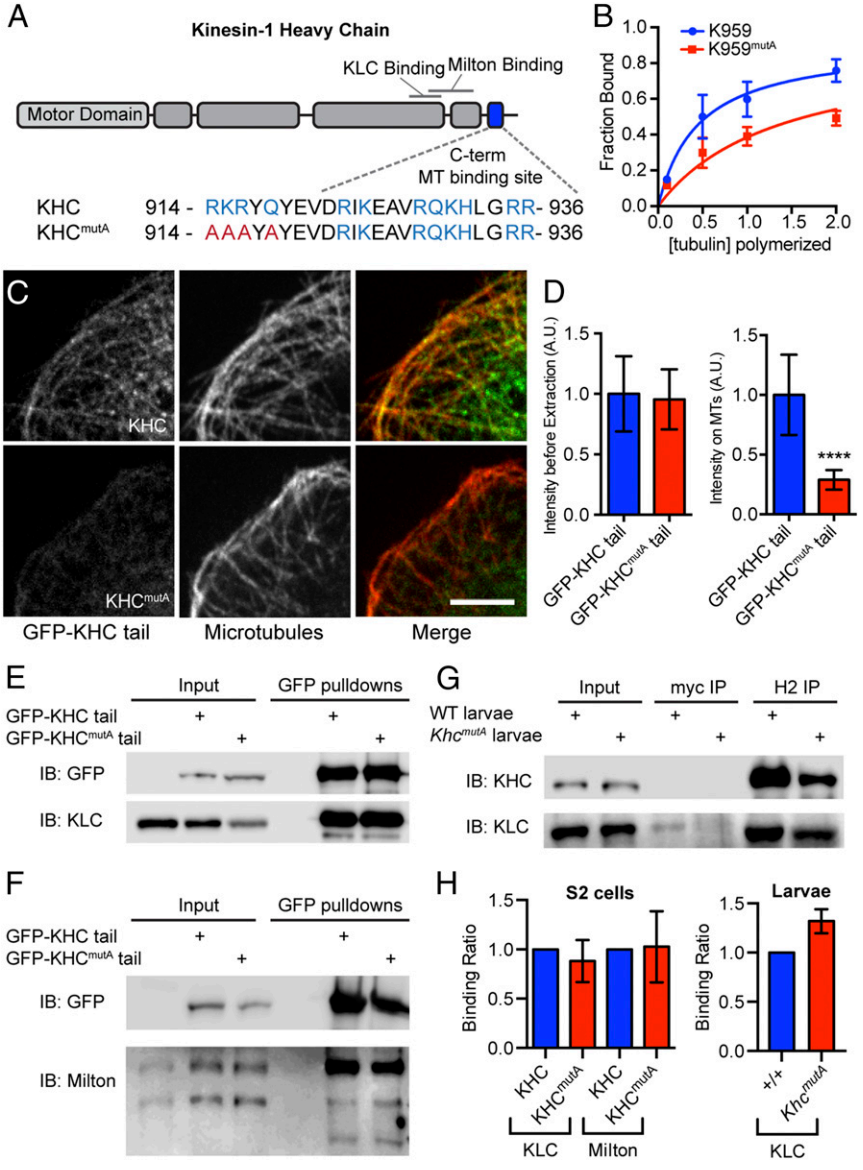


**Fig. 1.** Mutation of the C-terminal MT-binding site of KHC reduces affinity for MTs but does not affect cargo adapter binding. (*A*) Schematic diagram of KHC depicting the C-terminal MT-binding site and binding sites for cargo adapters (KLC and Milton). The amino acid sequences of the C-terminal MT-binding site and a quadruple-alanine mutation (KHC$^{mutA}$) are depicted. (*B*) Binding curves of purified wild-type or KHC$^{mutA}$ tail fragments (amino acids 844–959; called K959 and K959$^{mutA}$, respectively) with MTs in vitro. K959 binds MTs with $K_d = 0.44 \pm 0.08$ μM, and K959$^{mutA}$ tail binds with $K_d = 1.37 \pm 0.16$ μM (both represent average ± SD). These values were obtained from three independent experiments. Error bars indicate SEM. (*C*) Triton-extracted and fixed *Drosophila* S2 cells expressing GFP fusions of either wild-type KHC or KHC$^{mutA}$ tail (residues 345–975) and stained for α-tubulin. Note that KHC tail extensively decorates MTs, whereas KHC$^{mutA}$ tail is mostly removed by detergent extraction. (Scale bar, 5 μm.) (*D*) Intensity of GFP tail before extraction and after extraction along MTs. GFP-KHC$^{mutA}$ tail displayed significantly less accumulation along MTs. Before extraction: GFP-KHC tail, $n = 29$; GFP-KHC$^{mutA}$ tail, $n = 49$; after extraction: GFP-KHC tail, $n = 39$; GFP-KHC$^{mutA}$ tail, $n = 45$. ****$P < 0.0001$; Mann–Whitney test. Error bars indicate 95% confidence interval (CI). A.U., arbitrary units. (*E* and *F*) Pull-down of control, GFP-KHC tail, and GFP-KHC$^{mutA}$ tail from S2 cells stably expressing the constructs. KLC and mitochondrial adapter Milton both bind to GFP-KHC tail and GFP-KHC$^{mutA}$ tail. Multiple bands in the anti-Milton blot represent different splice isoforms. IB, immunoblot. (*G*) Coimmunoprecipitation of KHC from extracts of +/+ and *Khc$^{mutA}$* larvae. Negative control immunoprecipitations (IPs) were performed using a myc monoclonal antibody and KHC IPs were performed using a KHC monoclonal antibody, H2. Both wild-type KHC and KHC$^{mutA}$ pulled down KLC. (*H*) Quantification of cargo adapter binding. The ratio of cargo adapter to KHC signal was quantified from more than three pull-down or IP experiments for each condition. The affinity of KLC or Milton for KHC was comparable in control and KHC$^{mutA}$ extracts from either S2 cells or larval extracts. Error bars indicate 95% CI.

(Fig. S1 *A* and *B*). These results demonstrate that the C-terminal MT-binding site of KHC is necessary for MT sliding in S2 cells.

Next, we wanted to test whether this C-terminal MT-binding site was sufficient to slide MTs when coupled to a motor domain. We used a chimeric motor protein consisting of the motor domain of Unc104/kinesin-3 and a leucine zipper for dimerization (called UncLZ) (23). We fused this chimeric motor to the C terminus of KHC (amino acids 905–975), including the MT-binding site, creating UncLZ-Ktail (Fig. 2*A*). We found that UncLZ-Ktail was as effective at MT sliding as endogenous kinesin-1. Introduction of the quadruple-alanine mutations to the UncLZ-Ktail construct (UncLZ-Ktail$^{mutA}$) significantly reduced the ability of the chimera to slide MTs (Fig. 2*C* and Movie S2). We also found that after F-actin depolymerization, UncLZ-Ktail could generate processes comparable to control, whereas UncLZ and UncLZ-Ktail$^{mutA}$ could not (Fig. S1*B*). Overall, these data demonstrate that the C-terminal MT-binding site of KHC is a necessary and sufficient binding site that allows kinesin-1 to bind and slide MTs in *Drosophila* S2 cells. This mechanism is likely conserved in mammals because the MT-binding site itself is highly conserved (Fig. S2*A*) and expression of human KHC rescues MT sliding and process formation in *Drosophila* S2 cells depleted of endogenous kinesin-1 (Fig. S2 *B*–*E*).

**KHC$^{mutA}$ Does Not Affect Organelle Transport or Adapter Binding in S2 Cells.** To determine whether KHC$^{mutA}$ supports normal cargo transport, we first tested whether KHC$^{mutA}$ binds the known cargo adapters kinesin-1 light chain (KLC; used for transport of many kinesin-1 cargoes) (24) and Milton (used as an adapter for mitochondria transport) (25). Using S2 cell lines stably expressing GFP-tagged KHC or KHC$^{mutA}$ tail, we performed GFP pull-downs and probed pelleted proteins using antibodies against these

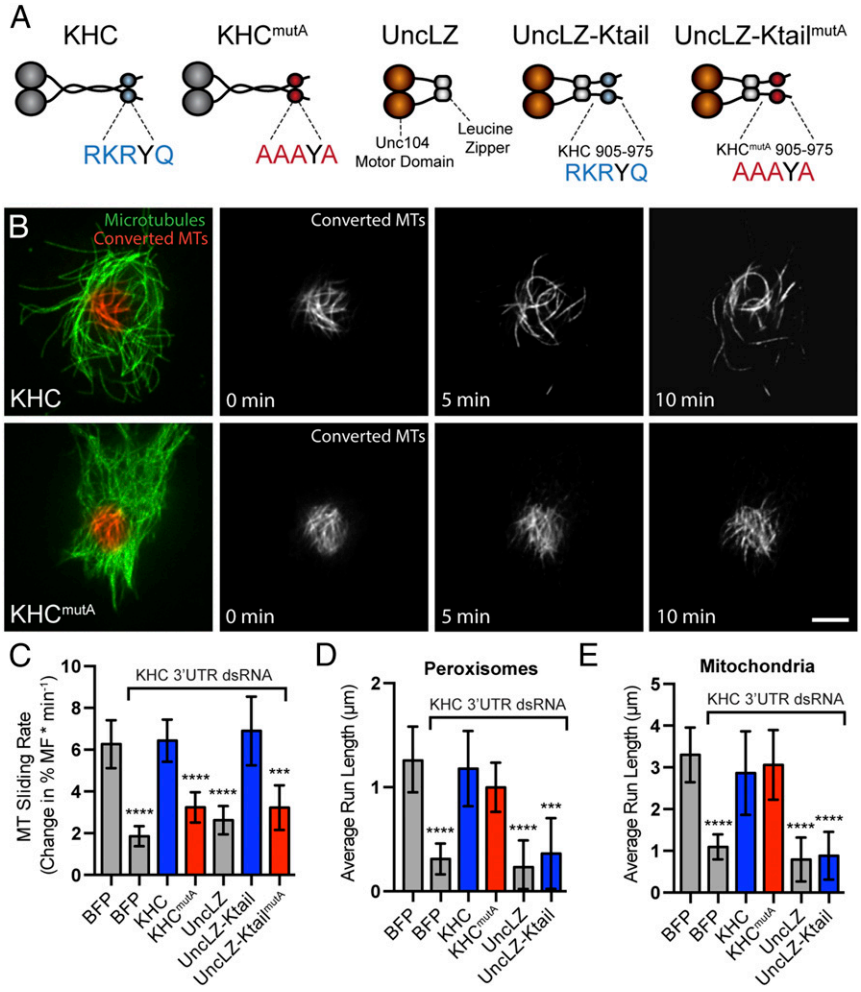


**Fig. 2.** KHC$^{mutA}$ cells displayed impaired MT sliding but normal mitochondria and peroxisome transport. (*A*) Schematic diagrams of constructs expressed after endogenous KHC knockdown. (*B*) S2 cells expressing photoconvertible tdEOS-tagged α-tubulin and KHC or KHC$^{mutA}$. Endogenous KHC was depleted by dsRNA targeting the 3′-UTR region. Photoconverted MT segments are depicted in red, and unconverted MTs are depicted in green. Photoconverted segments were tracked over time. Note that KHC$^{mutA}$ moves MTs slower than wild-type KHC (Movie S1). (Scale bar, 5 μm.) (*C*) MT sliding was quantified by segmenting MTs and determining the gross rate of MT movement outside of the initial converted zone (more detail is provided in *Materials and Methods*). KHC$^{mutA}$ displayed significantly reduced MT sliding activity compared with KHC. A chimeric motor containing the motor domain of kinesin-3/Unc104 fused to the C terminus of KHC (amino acids 905–975) rescued sliding, whereas KHC$^{mutA}$ alanine substitutions in this construct prevented this rescue (Movie S2) BFP, $n = 35$; BFP + KHC dsRNA, $n = 29$; KHC, $n = 38$; KHC$^{mutA}$, $n = 46$; UncLZ, $n = 17$; UncLZ-Ktail, $n = 25$; UncLZ-Ktail$^{mutA}$, $n = 27$. $^{**}P = 0.001$, $^{***}P = 0.0006$, $^{****}P < 0.0001$; Mann–Whitney test. Error bars indicate 95% CI. (*D* and *E*) Average peroxisome and mitochondria run length was assayed after expression of each construct. KHC and KHC$^{mutA}$ were both able to rescue cargo transport after endogenous KHC knockdown (Movies S3 and S4). Chimeric motors were unable to engage in peroxisome and mitochondria transport. (*D*) BFP, $n = 41$; BFP + KHC dsRNA, $n = 50$; KHC, $n = 30$; KHC$^{mutA}$, $n = 37$; UncLZ, $n = 13$; UncLZ-Ktail, $n = 13$. $^{***}P = 0.0003$, $^{****}P < 0.0001$; Mann–Whitney test. Error bars indicate 95% CI. (*E*) GFP, $n = 33$; GFP + KHC dsRNA, $n = 42$; KHC, $n = 21$; KHC$^{mutA}$, $n = 17$; UncLZ, $n = 17$; UncLZ-Ktail, $n = 16$. $^{****}P < 0.0001$; Mann–Whitney test. Error bars indicate 95% CI.

adapters. We quantified the ratio of adapter to KHC signal and found that KHC$^{mutA}$ maintained normal affinity for both KLC and Milton (Fig. 1 *E*, *F*, and *H*). Additionally, to determine if similar interactions occurred in vivo, we immunoprecipitated KHC or KHC$^{mutA}$ from flies (a description of flies expressing KHC$^{mutA}$ is provided in *Genomic Replacement of* Khc *with* Khc$^{mutA}$ *Reduces* Drosophila *Viability*) and found that both interacted with KLC equivalently (Fig. 1 *G* and *H*).

Although KHC$^{mutA}$ was able to bind cargo adapters, we wondered whether this mutant could transport organelles. We assayed the transport of two kinesin-1–dependent cargoes: peroxisomes, which use KLC to bind KHC (26), and mitochondria, which use the adapter Milton (25). We monitored peroxisome transport using a GFP-tagged peroxisome-targeting sequence (GFP-SKL) (27) and mitochondria transport using a fluorescent dye (MitoTracker Red). KHC and KHC$^{mutA}$ both rescued peroxisome and mitochondria transport in S2 cells after dsRNA depletion of endogenous KHC (Fig. S3 *A* and *E* and Movies S3 and S4). We quantified the average run length (Fig. 2 *D* and *E*) and velocity (Fig. S3 *D* and *H*) of peroxisomes and mitochondria (details are provided in *Materials and Methods*). No significant difference could be detected between organelles transported by KHC and KHC$^{mutA}$. Additionally, KHC$^{mutA}$ maintained a normal distribution of organelle run lengths and velocities compared with wild-type KHC (Fig. S3 *B*, *C*, *F*, and *G*). These results demonstrate that KHC$^{mutA}$ supports normal transport of peroxisomes and mitochondria. We also tested the ability of the sliding-competent UncLZ constructs to transport peroxisomes and mitochondria. Expression of UncLZ or UncLZ-Ktail did not rescue peroxisome or mitochondria run lengths after kinesin-1 knockdown (Fig. 2 *D* and *E*), indicating that organelle transport and MT sliding are two independent functions of kinesin-1. Overall, these data demonstrate that KHC$^{mutA}$ is able to bind and transport peroxisomes and mitochondria, suggesting that the mutation impairs MT sliding but has no effect on KLC-dependent transport or mitochondria transport.

**Genomic Replacement of *Khc* with *Khc$^{mutA}$* Reduces *Drosophila* Viability.** Kinesin-1–null phenotypes are thought to be due to organelle transport defects in the nervous system (28); however, MT sliding has not been examined. To test the role of MT sliding, we generated genomic-replacement KHC$^{mutA}$ flies, called *Khc$^{mutA}$*, using genome engineering (29) and φC31 site-specific recombination (30, 31). The endogenous kinesin-1 locus was replaced by a genomic kinesin-1 construct containing the MT-binding site mutations (KHC$^{mutA}$) (Fig. S4 *A* and *B*). As a control, wild-type kinesin-1 was also knocked-in to the endogenous locus, generating *Khc$^{wt}$*; this line is viable and fertile, and displays no obvious phenotypes. We determined by Western blot that KHC levels in *Khc$^{mutA}$* flies are comparable to *Khc$^{wt}$* and control flies (Fig. 3*A*), demonstrating that the knock-in method does not perturb KHC levels. We next assayed viability in homozygous *Khc$^{mutA}$* flies. *Khc$^{mutA}$* offspring from *Khc$^{mutA}$*/+ parents displayed 49.6% lethality before adulthood (Fig. 3*B*). However, because KHC is maternally loaded in embryos (13, 14), *Khc$^{mutA}$*/+ mothers deposit wild-type kinesin-1 mRNA and proteins into *Khc$^{mutA}$* embryos, potentially allowing many to survive throughout development. To observe earlier effects of *Khc$^{mutA}$*, we eliminated the maternal contribution of wild-type KHC by crossing *Khc$^{mutA}$* females to *Khc$^{mutA}$*/+ males. Strikingly, 89.4% of *Khc$^{mutA}$* offspring died before adulthood, with the strongest effect in the embryo (Fig. 3*B*). These results suggest that MT sliding by both maternal and zygotic KHC is important for normal development.

Interestingly, *Khc$^{mutA}$*/+ flies from the same crosses also displayed reduced viability (39.9% died from *Khc$^{mutA}$*/+ mothers and 63.9% died from *Khc$^{mutA}$* mothers). Because kinesin-1 molecules contain two heavy chains, many kinesin-1 dimers in *Khc$^{mutA}$*/+ animals are likely KHC/KHC$^{mutA}$ heterodimers. The lethality observed in *Khc$^{mutA}$*/+ animals may suggest that KHC$^{mutA}$ can exert a dominant-negative effect and that mixed KHC/KHC$^{mutA}$ heterodimers cannot bind MTs as efficiently as wild-type homodimers. Alternatively, this effect may be caused by earlier patterning defects caused by the maternally contributed *Khc$^{mutA}$*.

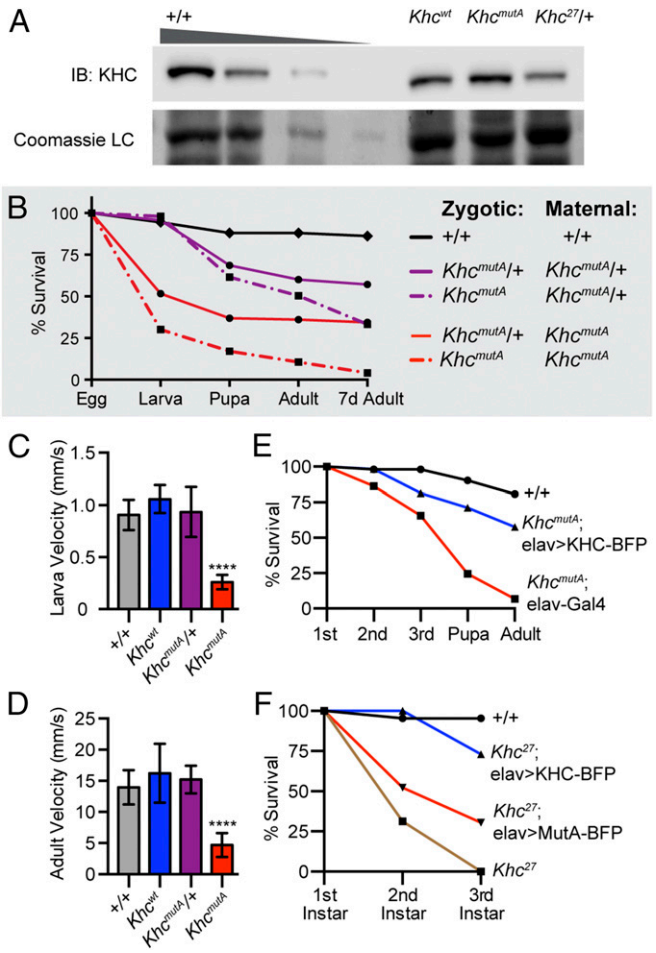


**Fig. 3.** Mutation of the C-terminal MT-binding site of kinesin-1 resulted in locomotion and viability defects in *Drosophila*. (*A*) Western blot comparing KHC protein levels in +/+, *Khc$^{wt}$*, *Khc$^{mutA}$*, and *Khc$^{27}$*/+ flies. Protein extract from +/+ flies was loaded at 20 μg, 10 μg, 5 μg, and 2 μg, whereas other genotypes were loaded at 20 μg. Samples were probed with a KHC antibody and stained with Coomassie for a loading control (LC). *Khc$^{wt}$* (genomic wild-type KHC knock-in) and *Khc$^{mutA}$* (genomic KHC$^{mutA}$ knock-in) flies displayed similar KHC levels to +/+. As a control, *Khc$^{27}$*/+ fly extracts were probed; these extracts contained 50% KHC level, as expected. Western blot intensity (average ± SD; A.U.): 20 μg +/+, 1.00 ± 0.00; 10 μg +/+, 0.48 ± 0.30; 5 μg +/+, 0.19 ± 0.19; 2.5 μg +/+, 0.02 ± 0.03; *Khc$^{wt}$*, 0.92 ± 0.24; *Khc$^{mutA}$*, 0.88 ± 0.05; and *Khc$^{27}$*/+, 0.47 ± 0.09. (*B*) Survival curve of *Khc$^{mutA}$* and *Khc$^{mutA}$*/+ flies from homozygous or heterozygous parents. *Khc$^{mutA}$* flies from homozygous parents displayed the strongest lethality phenotype. +/+, $n = 109$; *Khc$^{mutA}$*/+ (zygotic; zyg) *Khc$^{mutA}$*/+ (maternal; mat), $n = 488$; *Khc$^{mutA}$* (zyg) *Khc$^{mutA}$*/+ (mat), $n = 250$; *Khc$^{mutA}$*/+ (zyg) *Khc$^{mutA}$* (mat), $n = 122$; *Khc$^{mutA}$* (zyg) *Khc$^{mutA}$* (mat), $n = 123$. (*C* and *D*) Motility rates of third-instar larvae and adult flies. *Khc$^{mutA}$* animals moved significantly slower than wild-type and heterozygous animals (Movies S5 and S6). (*C*) +/+, $n = 14$; *Khc$^{wt}$*, $n = 12$; *Khc$^{mutA}$*/+, $n = 19$; *Khc$^{mutA}$*, $n = 19$. (*D*) +/+, $n = 13$; *Khc$^{wt}$*, $n = 18$; *Khc$^{mutA}$*/+, $n = 20$; *Khc$^{mutA}$*, $n = 21$. ****$P < 0.0001$; Mann–Whitney test. Error bars indicate 95% CI. (*E*) Expression of wild-type KHC in neurons partially rescued *Khc$^{mutA}$* lethality. +/+, $n = 52$; *Khc$^{mutA}$*, *elav-Gal4*, $n = 73$; *Khc$^{mutA}$*, *elav > KHC-BFP*, $n = 59$. (*F*) Expression of wild-type KHC in neurons delayed lethality in KHC protein-null *Khc$^{27}$* larvae (blue line). Expression of KHC$^{mutA}$ was not as effective (red line). All *Khc$^{27}$* animals died before pupation regardless of KHC expression. +/+, $n = 43$; *Khc$^{27}$*, $n = 15$; *Khc$^{27}$*, *elav > KHC-BFP*, $n = 37$; *Khc$^{27}$*, *elav > KHC$^{mutA}$-BFP*, $n = 23$.

Previous studies reported that kinesin-1–null larvae and temperature-sensitive mutant adults display locomotion defects (13).

To determine if MT sliding contributes to these defects, we assayed crawling and walking velocities in $Khc^{mutA}$ larvae and adults (32). $Khc^{mutA}$ larvae displayed severe locomotion defects, with crawling velocities significantly slower than control larvae (Fig. 3*C* and Movie S5). Some larvae displayed a classic tail-flipping locomotion defect, caused by dorsal-ventral paralysis that disrupts normal peristaltic muscle contractions (28). $Khc^{mutA}$ adults also moved significantly slower than control (Fig. 3*D* and Movie S6). These results suggest that loss of kinesin-1–based MT sliding causes locomotion defects.

Our laboratory has demonstrated that kinesin-1 is required for neurite outgrowth and axon regeneration in cultured primary neurons (7, 8), prompting us to test whether $Khc^{mutA}$ lethality is caused by defects in the nervous system. Our strategy was to rescue MT sliding in neurons using the Gal4/UAS tissue-specific expression system and then to assay viability. For these experiments, we generated third-chromosome transgenes encoding *UASp-KHC-BFP* or *UASp-KHC$^{mutA}$-BFP*. Expression of wild-type KHC in the nervous system using the pan-neuronal driver *elav* (33, 34) partially rescued the viability defect in $Khc^{mutA}$ flies (Fig. 3*E*), suggesting neuronal MT sliding is important in vivo. However, because the rescue was partial, MT sliding is likely important in other tissues as well. In support of this idea, an accompanying study demonstrates the role of MT sliding in cytoplasmic streaming and polarity determination during *Drosophila* oogenesis (35). We also tested whether we could rescue lethality in $Khc^{27}$ flies, a kinesin-1–null allele (14). Neuronal expression of wild-type KHC, but not KHC$^{mutA}$, delayed lethality in $Khc^{27}$ larvae (Fig. 3*F*); however, all $Khc^{27}$ animals died before pupation, regardless of transgenic expression. Together, these data highlight the importance of MT sliding in the nervous system.

**$Khc^{mutA}$ Neurons Exhibit Decreased MT Sliding and Axon Outgrowth but Maintain Normal Peroxisome and Mitochondria Transport.** We next tested whether $Khc^{mutA}$ flies displayed reduced MT-sliding rates as demonstrated in *Drosophila* S2 cells (Fig. 2). We assayed MT-sliding rates in neurons because neuronal MT sliding appears to be important for survival (Fig. 3 *E* and *F*). To avoid the effect of maternally loaded KHC, we isolated and cultured neurons from dissociated brains of third-instar larvae (8), when maternal load is minimal (13). To assay MT sliding, MTs were photoconverted in the cell bodies of newly cultured neurons expressing *elav > tdEOS-tubulin* (7). $Khc^{mutA}$ neurons displayed significantly reduced MT sliding compared with control (Fig. 4 *A* and *B* and Movie S7). $Khc^{mutA}$/+ neurons exhibited an intermediate sliding rate, supporting the idea that $Khc^{mutA}$ might reduce MT sliding through dominant-negative inhibition (Fig. 4*B*).

To test whether mutant KHC can maintain normal organelle transport in $Khc^{mutA}$ neurons, we assayed mitochondria transport in cultured neurons using MitoTracker Red. No significant difference was observed between mitochondria run lengths and velocities in control and $Khc^{mutA}$ neurons (Fig. 4*C*, Fig. S5 *A–D* and Movie S8). Additionally, we wanted to test whether KHC from $Khc^{mutA}$ flies could interact with KLC, which acts as a general adapter for many different kinesin-1 cargoes. We immunoprecipitated wild-type KHC and KHC$^{mutA}$ from +/+ and $Khc^{mutA}$ larval extracts. We probed extracts with an anti-KLC antibody and found that both wild-type and mutant KHC interacted with KLC (Fig. 1*F*). Furthermore, we assayed peroxisome transport in cultured neurons isolated from control and $Khc^{mutA}$ larvae expressing *elav > GFP-SKL*. No significant difference was observed between peroxisome run lengths and velocities in control and $Khc^{mutA}$ neurons (Fig. 4*D*, Fig. S5 *E–H*, and Movie S9). These results demonstrate that $Khc^{mutA}$ flies display defects in MT sliding but maintain normal peroxisome and mitochondria transport.

Based on our previous studies (6–9, 36), we hypothesized that kinesin-1–based MT sliding drives axon outgrowth. Although kinesin-1 has been implicated in axon outgrowth previously (37, 38), the mechanism has not been elucidated and the role of MT sliding is not yet clear. To test our hypothesis of sliding-based outgrowth directly, we cultured $Khc^{mutA}$ neurons for 48 h before fixing and staining for MTs and F-actin. Strikingly, $Khc^{mutA}$ neurons displayed significantly shorter axons compared with control neurons (Fig. 4 *E* and *F*), suggesting that MT sliding is required for axon outgrowth. $Khc^{mutA}$/+ neurons also displayed an intermediate axon outgrowth phenotype, consistent with the intermediate sliding and lethality phenotypes observed previously (Figs. 3*B* and 4*B*).

To test our hypothesis of sliding-based axon outgrowth further, we generated transgenic flies containing the Unc104/kinesin-3 chimeric motor, UncLZ-Ktail, which slides MTs but cannot transport organelles (Fig. 2). We found that expression of UncLZ-Ktail in $Khc^{mutA}$ neurons rescued the shortened axon phenotype and generated axons that were even longer than control (Fig. 4 *G* and *H*). Expression of the control chimera, UncLZ, or mutated chimera, UncLZ-Ktail$^{mutA}$, did not rescue axon outgrowth in $Khc^{mutA}$ neurons. These experiments demonstrate that kinesin-1–based MT sliding drives axon outgrowth in *Drosophila* neurons.

**$Khc^{mutA}$ Animals Exhibit Reduced MT Sliding and Axon Outgrowth Defects in Vivo.** Although MT sliding has been observed in tissue culture cells and cultured neurons, no study has yet demonstrated that MT sliding can occur in an animal. This lack of demonstration is likely because photoconversion experiments in vivo are difficult and MT sliding is only observed during active outgrowth (7). To test whether sliding occurs in neurons in vivo, we imaged sensory neurons expressing the photoconvertible probe, tdMaple3-tubulin (35), driven by neur-Gal4 (39) in the anterior and posterior dorsocentral macrochaetae of intact pupae (40) (Fig. 5*A*). To visualize MTs during a stage of active axon outgrowth when MT sliding occurs, we imaged these sensory neurons 20–22 h after puparium formation, during the initial axon growth stage. MTs were photoconverted at the proximal axon to image MT sliding. We found robust MT sliding in these neurons during 20-min time lapses (Fig. 5*B* and Movie S10). To test if this MT sliding was kinesin-1–based, we imaged MT sliding in sensory neurons in $Khc^{mutA}$ animals. $Khc^{mutA}$ neurons in intact pupae exhibited greatly reduced MT sliding compared with control (Fig. 5*B*). Due to low signal and high background, the in vivo images of MTs were challenging to analyze using our standard method. To overcome this obstacle, we quantified the percentage of fluorescence leaving the initial converted zone after photoconversion as an indirect measure of MT sliding. We found that significantly more fluorescence left the initial converted zone in control neurons compared with $Khc^{mutA}$ neurons (Fig. 5*C*). It should be noted that these results quantify total photoconverted tdMaple3-tubulin signal. Although the majority of tdMaple3-tubulin is likely incorporated in MTs, these measurements cannot be directly compared with the quantification of MT sliding shown in Figs. 2 and 4. Overall, these results demonstrate that robust MT sliding occurs in vivo and that kinesin-1 drives this sliding using the same MT-binding site as has been characterized in S2 cells and in cultured neurons.

We next tested whether the decrease in MT sliding observed in $Khc^{mutA}$ animals resulted in axon phenotypes in vivo. We examined the classic photoreceptor axon-targeting pattern in the optic lobes of third-instar larvae. Axons extend from the cell bodies of photoreceptor neurons in the eye disc and converge together into the optic stalk. The axons encounter the lamina of the optic lobes and form a retinotopic pattern (41) (Fig. 5*D*). We dissected brains from third-instar $Khc^{mutA}$ larvae and fixed and stained for Futsch, a neuron-specific MT-associated protein, to reveal the axon patterning of the photoreceptor neurons (Fig. 5*E*). Compared with the control, we found that $Khc^{mutA}$ photoreceptor neurons displayed a severe phenotype: Axons targeting to the lamina were mostly lost (Fig. 5*E*). The optic stalk in $Khc^{mutA}$ was also dramatically thinner compared with control, suggesting that many axons were severely shortened and could

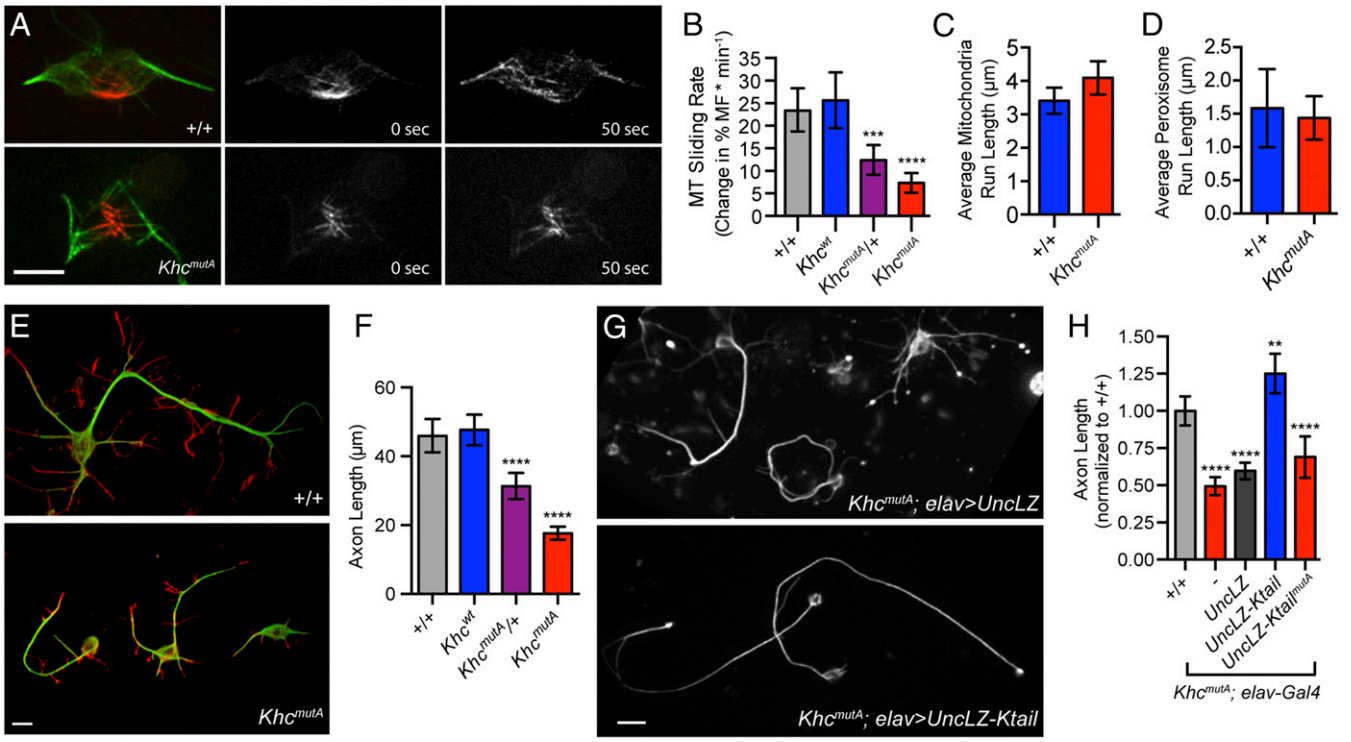


**Fig. 4.** Neurons from $Khc^{mutA}$ larvae displayed reduced MT sliding and axon length but maintained normal mitochondria and peroxisome transport. (*A*) Primary neurons from +/+ and $Khc^{mutA}$ larvae expressing *elav* > tdEOS-tagged α-tubulin. Photoconverted MTs are depicted in red, and unconverted MTs are depicted in green. Note that fewer MTs leave the photoconverted zone in the $Khc^{mutA}$ neuron (Movie S7). (Scale bar, 5 μm.) (*B*) Quantification of MT sliding activity. $Khc^{mutA}$ homozygous and heterozygous neurons displayed reduced MT sliding compared with control neurons. +/+, $n = 41$; $Khc^{wt}$, $n = 31$; $Khc^{mutA}$/+, $n = 26$; $Khc^{mutA}$, $n = 27$. ***$P = 0.0012$, ****$P < 0.0001$; Mann–Whitney test. Error bars indicate 95% CI. (*C* and *D*) Mitochondria and peroxisome transport was assayed in primary neurons using a mitochondria dye, MitoTracker Red, or a transgene, *UASp-GFP-SKL*. No significant difference in average mitochondria or peroxisome run lengths was observed between +/+ and $Khc^{mutA}$ (Movies S8 and S9). Mitochondria: +/+, $n = 51$; $Khc^{mutA}$, $n = 44$. Peroxisomes: +/+, $n = 23$; $Khc^{mutA}$, $n = 31$. Error bars indicate 95% CI. (*E* and *F*) Neurons were fixed and stained 48 h after plating. MTs are depicted in green, and F-actin is depicted in red. $Khc^{mutA}$ neurons displayed significantly shorter axons than control. $Khc^{mutA}$/+ neurons displayed an intermediate phenotype. +/+, $n = 78$; $Khc^{wt}$, $n = 83$; $Khc^{mutA}$/+, $n = 92$; $Khc^{mutA}$, $n = 121$. ****$P < 0.0001$; Mann–Whitney test. Error bars indicate 95% CI. (Scale bar, 5 μm.) (*G* and *H*) UncLZ or UncLZ-Ktail expression was driven in $Khc^{mutA}$ neurons by *elav-Gal4*. Neurons were fixed and stained using an antibody against α-tubulin 48 h after plating. Axon length was measured and normalized to control neurons. Expression of UncLZ-Ktail rescued axon outgrowth in $Khc^{mutA}$ neurons and resulted in axons significantly longer than control neurons. Expression of UncLZ or UncLZ-Ktail$^{mutA}$ in $Khc^{mutA}$ neurons did not rescue axon length. +/+, $n = 104$; $Khc^{mutA}$: *elav-Gal4*, $n = 120$; $Khc^{mutA}$: *elav* > *UncLZ*, $n = 168$; $Khc^{mutA}$: *elav* > *UncLZ-Ktail*, $n = 89$; $Khc^{mutA}$: *elav* > *UncLZ-Ktail*$^{mutA}$, $n = 90$. **$P = 0.0036$, ****$P < 0.0001$; Mann–Whitney test. Error bars indicate 95% CI. (Scale bar: *G*, 5 μm.)

not even reach the optic stalk. These phenotypes were highly penetrant and seen in a majority of $Khc^{mutA}$ larvae (Fig. 5*F*). We attempted to rescue this phenotype by expressing the Unc104/kinesin-3 chimera (UncLZ-Ktail), which can slide MTs but cannot transport organelles. We found that neuronal expression of UncLZ-Ktail in $Khc^{mutA}$ animals rescued axon outgrowth and patterning of photoreceptor neurons in a majority of animals (Fig. 5 *E* and *F*). The thinning of the optic stalk was also rescued, suggesting that more axons were able to extend out from the eye disc. Conversely, expression of UncLZ-Ktail$^{mutA}$ in $Khc^{mutA}$ larvae did not rescue this axon innervation defect. These results demonstrate that kinesin-1–based MT sliding is required for axon outgrowth not only in culture but also in vivo.

***$Khc^{mutA}$* Larvae Display No Synaptotagmin Aggregates and Mild Cysteine String Protein Aggregates in Segmental Nerves.** Previous studies have observed swellings along the axon shafts of the segmental nerve motor neurons in *Khc* mutants (28). These swellings contain accumulations of membrane organelles, such as synaptotagmin (SYT), cysteine string protein (CSP), and mitochondria, which are unable to move to the axon tip in the absence of kinesin-1. We wondered if similar vesicle aggregates could be observed in $Khc^{mutA}$ animals. As a control, we stained the segmental nerves of control larvae and KHC-depleted larvae (*elav* > *Khc RNAi*) using a SYT antibody. We found, as previously reported, that KHC depletion (*elav* > *Khc RNAi*) resulted in numerous large aggregates of SYT in segmental nerves (28, 42). Conversely, both +/+ and $Khc^{mutA}$ larvae displayed no observable SYT aggregates in the segmental nerves (Fig. S6*A*). These results were quantified by measuring the sum pixel intensity of SYT aggregates in each genotype (Fig. S6*B*).

Next, we stained segmental nerves using a CSP antibody. As expected, based on previous studies, CSP robustly accumulated in segmental nerves after kinesin-1 depletion in *elav* > *Khc RNAi* larvae (28). In contrast, the segmental nerves of $Khc^{mutA}$ larvae displayed mild accumulation of CSP, whereas control larvae displayed no accumulations (Fig. S7 *A* and *B*). Because the kinesin-1–binding protein Unc-76 is important for CSP transport (43), we wondered if the quadruple-alanine mutation in $Khc^{mutA}$ affected the binding site of Unc-76, which is near the C-terminal MT-binding site and IAK domain (44). To test this possibility, we performed pull-downs using GFP-KHC tail and GFP-KHC$^{mutA}$ tail S2 cell lines. We found that although GFP-KHC$^{mutA}$ tail interacted with Unc-76, this binding was decreased to ∼50% of the wild-type level (Fig. S7 *C* and *D*). We attempted to recapitulate the $Khc^{mutA}$ CSP phenotype by decreasing either kinesin-1 or Unc-76 protein levels using protein-null heterozygotes, $Khc^{27}$/+ and *Df(Unc-76)*/+. We found that many $Khc^{27}$/+ and *Df(Unc-76)*/+ animals

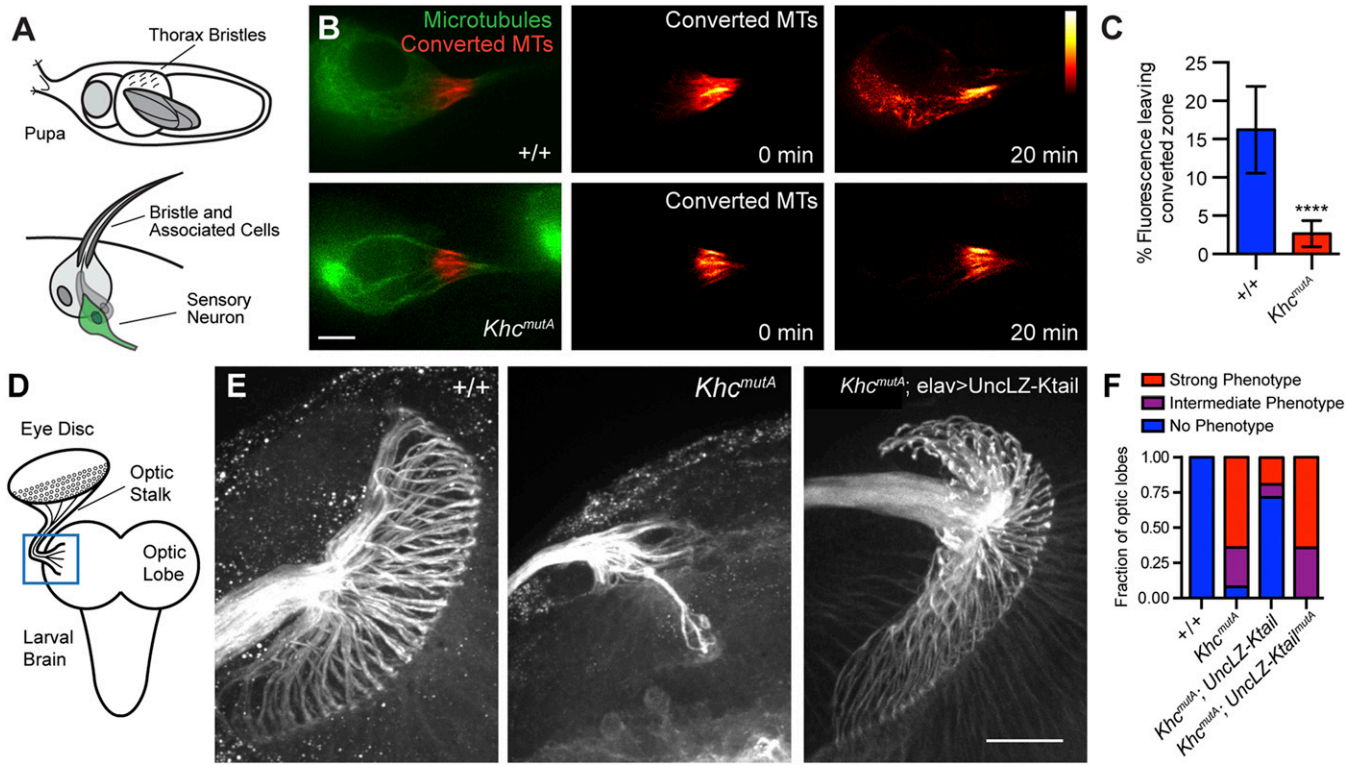


**Fig. 5.** Neurons in intact $Khc^{mutA}$ animals displayed reduced MT sliding and axon defects in the optic lobes. (*A*) Diagram of *Drosophila* pupa and bristle structure. Large sensory bristles called macrochaetae coat the surface of the *Drosophila* pupa (*Top*). These structures each contain a sensory neuron (green, *Bottom*), whose dendrite innervates the base of the bristle and whose axon grows deep into the thoracic ganglion. (*B*) MT sliding was assayed in macrochaetae sensory neurons expressing $neur^{A101} > tdMaple3\text{-}tubulin$. Photoconverted MTs are depicted in red, and unconverted MTs are depicted in green. A red heat map was used to display converted MTs at 0 and 20 min. Note that $Khc^{mutA}$ neurons display drastically less MT sliding (Movie S10). (Scale bar, 5 μm.) (*C*) Percentage of fluorescence leaving the initial converted zone was quantified for +/+ and $Khc^{mutA}$ sensory neurons. Significantly less signal left the converted zone in $Khc^{mutA}$ neurons compared with control. +/+, $n = 20$; $Khc^{mutA}$, $n = 10$. $^{****}P < 0.0001$; Mann–Whitney test. Error bars indicate 95% CI. (*D*) Diagram of dissected third-instar larval brain. The optic stalk, which contains axons of photoreceptors neurons, connects the eye imaginal disc to the optic lobe of the brain. This interface was imaged (blue box). (*E*) Third-instar larval brains were fixed and stained with anti-Futsch antibody (a neuronal MT-associated protein). Axon terminals at the optic lobe display an extensive umbrella-like pattern in control larvae. This pattern is lost in a majority of $Khc^{mutA}$ larvae. Expression of the chimeric motor UncLZ-Ktail, capable of MT sliding but not organelle transport, rescued this phenotype in many $Khc^{mutA}$ animals. The chimera containing the $KHC^{mutA}$ mutation ($UncLZ\text{-}Ktail^{mutA}$) was unable to rescue this phenotype. (Scale bar, 20 μm.) (*F*) Graph depicts the fraction of optic lobes displaying no phenotype (blue), a strong phenotype (red), or an intermediate phenotype (purple). +/+, $n = 10$; $Khc^{mutA}$, $n = 25$; $Khc^{mutA}$: $elav > UncLZ\text{-}Ktail$, $n = 21$; $Khc^{mutA}$: $elav > UncLZ\text{-}Ktail^{mutA}$, $n = 14$.

displayed mild CSP accumulations (Fig. S7*B*). $Khc^{27}$/+ animals also displayed mild SYT accumulations, which were not observed in $Khc^{mutA}$ larvae (Fig. S6). Importantly, both $Khc^{27}$/+ and *Df(Unc-76)*/+ animals display no significant viability or locomotion defects (Fig. S7 *E–G*), although they display mild CSP accumulations in segmental nerves. $Khc^{mutA}$ animals, on the other hand, display both viability and locomotion defects (Fig. 3). These results suggest that the mild CSP accumulations observed in $Khc^{mutA}$ animals are likely not responsible for the observed phenotypes.

**MT Sliding Is Required for Dendritic Arborization.** A previous study has implicated kinesin-1 in dendritic branching in class IV dendritic arborization (da) sensory neurons (45). These neurons display complex arborization patterns and are easily imaged in intact third-instar larvae. Kinesin-1 and dynein-based transport of Rab5 vesicles was implicated in dendritic branching, but we wondered if MT sliding played a role in dendrite outgrowth. We generated $Khc^{mutA}$ flies expressing a GFP membrane marker in class IV neurons (*ppk > mCD8-GFP*) to image the overall morphology of the neurons. Class IV da neurons displayed a striking phenotype in $Khc^{mutA}$ larvae: The dendritic trees were greatly reduced with less arborization (Fig. 6*A*). Sholl analysis (46) demonstrated that $Khc^{mutA}$ arbors contain significantly fewer branches (Fig. 6*B*); additionally, the total dendrite length of $Khc^{mutA}$ neurons was reduced (Fig. 6*C*). Although $Khc^{mutA}$ larvae were slightly smaller than control, this finding could not account for the difference observed in dendritic arbors, because the size of abdominal segments in $Khc^{mutA}$ larvae was only 9.6% (segment A1) or 14.4% (segment A6) smaller than control when measured from anterior to posterior. We also examined the dendritic trees of class I neurons using *221-Gal4*. We observed reduced branching and shortened dendrites in class I da neurons in $Khc^{mutA}$ larvae (Fig. S8 *A–E*), suggesting that MT sliding may be a general mechanism for dendritic branching.

We wondered if these defects in dendritic branching had an effect on sensory processing and behavior. Class IV da neurons have been reported to detect noxious thermal (47) and mechanical stimuli (48, 49), triggering larvae to engage in escape behaviors to evade predators such as parasitoid wasps (50, 51). Previous studies have shown that noxious mechanical stimulation to the middle segments of third-instar larvae results in a reproducible, dorsal-ventral rolling escape behavior (51). Using this rolling behavior as an output, we assayed nociception in $Khc^{mutA}$ larvae. Although a majority of +/+ and $Khc^{wt}$ larvae responded to mechanical stimulation, less than half of $Khc^{mutA}$ larvae responded (Fig. 6*D*). This finding suggests that the reduction in dendritic arborization seen

in $Khc^{mutA}$ class IV da neurons partially desensitizes the larvae to noxious stimuli.

Next, we assayed the distribution of Rab5 vesicles in class IV da neurons to determine whether their transport was impaired, which might explain the reduced arborization. We found Rab5 vesicles in the distal branches of both control and $Khc^{mutA}$ larvae (Fig. 6*E*), suggesting no defects in Rab5 transport caused by $KHC^{mutA}$. This result is in contrast to the phenotypes observed in *Khc*-null animals, where class IV da neurons display very few Rab5 vesicles in distal dendrites and increased accumulation of Rab5 vesicles near the cell body (45). This accumulation of Rab5 vesicles near the cell body results in a striking proximal branching phenotype, which was also not observed in $Khc^{mutA}$ larvae. Time-lapse imaging of Rab5 transport in living, intact larvae also demonstrated that both anterograde and retrograde transport of Rab5 vesicles was unimpaired in $Khc^{mutA}$ animals (Fig. 6*F* and Movie S11). Altogether, these results demonstrate a previously unidentified role for kinesin-1–based MT sliding in dendritic arborization in vivo.

## Discussion

For decades, it has been known that kinesin-1 plays an important role in the nervous system. In vertebrates, knockout of the major kinesin-1 gene, KIF5B, results in embryonic lethality (52). In flies, kinesin-1–null mutants exhibit synaptic dysfunction, locomotion defects, paralysis, and eventual death before reaching pupal stages (13, 14). Kinesin-1 mutation results in an accumulation of synaptic proteins, such as SYT, in swellings along the axon shaft (28). These swellings contain both retrograde and anterograde motors and cargoes, and they are thought to act as traffic jams, blocking fast retrograde and anterograde transport (42). Axonal swellings in kinesin-1 mutants have been compared with pathological swellings observed in human diseases such as amyotrophic lateral sclerosis and spinal muscular atrophy, and were therefore hypothesized to be the primary cause of kinesin-1 mutant lethality. However, contrary to this traffic jam model, live imaging demonstrated that cargoes could robustly move through axonal swellings (53), suggesting that kinesin-1 mutant lethality may be more complicated than general defects in cargo transport.

We have previously shown that in addition to its role in cargo transport, kinesin-1 can transport MTs, resulting in MT sliding (6). These sliding MTs push on the plasma membrane and extend axons in cultured neurons during initial outgrowth and during regeneration after injury (7, 8). Because kinesin-1 is important for both fast axonal transport and MT-driven neurite outgrowth, the cause of early neurological phenotypes in kinesin-null animals is unclear. To determine the role of MT sliding, we needed to identify the mechanism of kinesin-1–based MT sliding and generate a mutant with reduced MT sliding.

Our hypothesis was that the nonmotor MT-binding site in the C terminus of kinesin-1 (15) acts as an MT adapter, allowing kinesin-1 to bind one MT and carry it as a cargo along the second MT, causing MT sliding. This C-terminal MT-binding site has been extensively characterized biochemically (16, 17), but its biological role was not clear. In this study, we created a mutation in the C-terminal MT-binding domain of KHC by substituting four charged residues with alanines (RKRYQ to AAAYA, called $KHC^{mutA}$). In agreement with the biochemical data on human KHC, this mutant has reduced affinity for MTs in vitro and in cells. Here, we demonstrate, for the first time to our knowledge, that the C-terminal MT-binding domain of KHC is required for cytoplasmic MT sliding. $KHC^{mutA}$ displayed significantly reduced MT sliding compared with wild-type KHC. Importantly, the ability of $KHC^{mutA}$ to bind many cargo adapters and transport cargoes was similar to wild-type KHC. This finding is in agreement with a study in *Caenorhabditis elegans*, which demonstrated that a similar mutation in the C-terminal MT-binding site of kinesin-1 did not affect mitochondria transport (11).

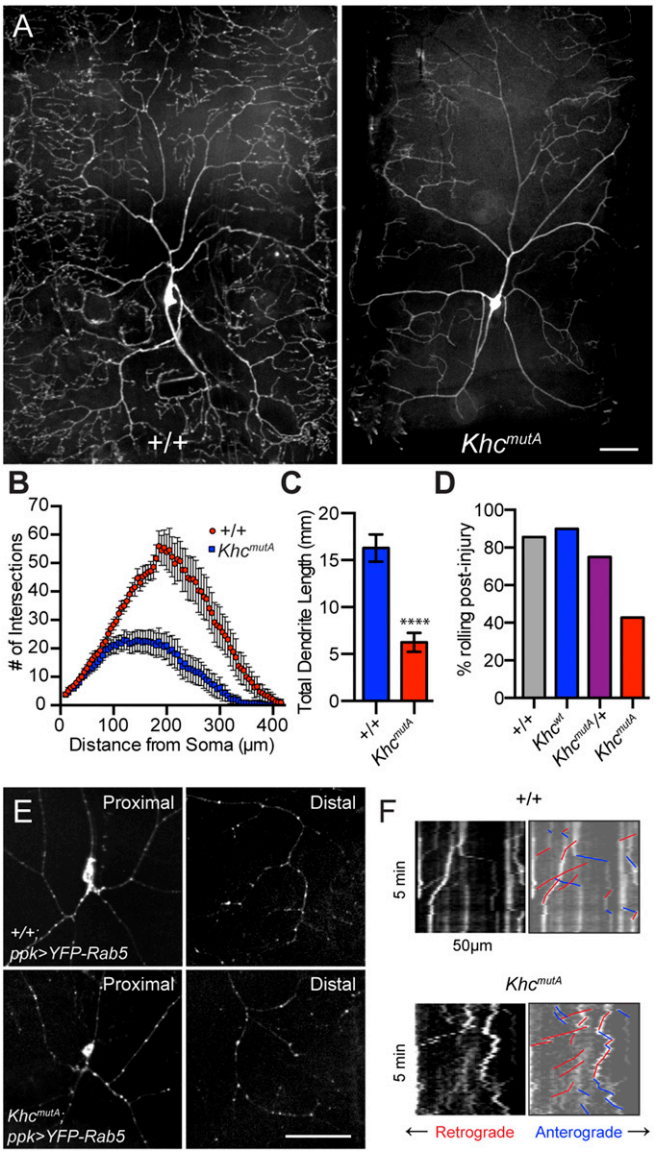


**Fig. 6.** MT sliding contributes to dendritic arborization in *Drosophila* da neurons. (*A*) Class IV da neurons imaged in segment A6 of control and $Khc^{mutA}$ larvae. Note the reduced arborization in the $Khc^{mutA}$ larva. (Scale bar, 50 μm.) (*B*) Sholl analysis indicated that $Khc^{mutA}$ neurons contain less complex dendritic trees. (*C*) Total dendrite length is also reduced in $Khc^{mutA}$ neurons compared with control. +/+, $n = 16$; $Khc^{mutA}$, $n = 24$. ****$P < 0.0001$; Mann–Whitney test. Error bars indicate 95% CI. (*D*) Stereotypical dorsal-ventral rolling behavior was assayed in *Drosophila* larvae after mechanical stimulation. A total of 42.9% of $Khc^{mutA}$ larvae responded to this stimulation, whereas 85.7% and 90% of +/+ and $Khc^{wt}$ larvae responded, respectively. +/+, $n = 7$; $Khc^{wt}$, $n = 10$; $Khc^{mutA}$/+, $n = 12$; $Khc^{mutA}$, $n = 28$. (*E*) Rab5 vesicles were visualized in class IV da neurons in +/+ and $Khc^{mutA}$ larvae using a transgene (*UASp-YFP-Rab5*). Rab5 vesicles were detected in proximal and distal dendrite arbors in +/+ and $Khc^{mutA}$ larvae. +/+, $n = 13$; $Khc^{mutA}$, $n = 12$. (Scale bar, 50 μm.) (*F*) Time-lapse images of Rab5 vesicles near the cell body of class IV da neurons were acquired in live +/+ and $Khc^{mutA}$ larvae. Kymographs of YFP-Rab5 time lapses from +/+ and $Khc^{mutA}$ larvae suggest that both genotypes support Rab5 transport. Retrograde transport events were colored red, and anterograde transport events were colored blue (Movie S11). +/+, $n = 7$; $Khc^{mutA}$, $n = 7$.

To determine the role of MT sliding in vivo, we replaced the genomic locus of kinesin-1 with our quadruple-alanine mutant, generating $Khc^{mutA}$ flies. We found that a majority of homozygous $Khc^{mutA}$ animals died before adulthood and larvae displayed locomotion

defects, as has been described in kinesin-1 mutants (13). Interestingly, mutation of many kinesin-1 cargo adapters, such as KLC, also results in locomotion defects (54). We speculate that defects in organelle transport may affect delivery of neurotransmitter-containing vesicles, whereas defects in MT sliding may affect neuronal wiring. Either of these defects will impair neuronal communication, potentially resulting in similar phenotypic outputs: locomotion defects and eventual lethality. In support of this idea, depletion of the MT-sliding regulator, Pavarotti/MKLP1, results in locomotion and viability defects (9).

Inhibition of MT sliding also resulted in additional phenotypes. $Khc^{mutA}$ adults are smaller, walk slowly, have trouble eclosing from the pupal case, and incessantly rub their legs together. The lethality observed in these flies seems to be largely caused by neuronal phenotypes, because neuron-specific expression of wild-type KHC greatly alleviated $Khc^{mutA}$ lethality. Additionally, we were able to delay lethality in kinesin-1-null $Khc^{27}$ larvae by neuronal expression of wild-type KHC, but not $KHC^{mutA}$. $Khc^{27}$ larvae with neuronal wild-type KHC expression appeared to have no progressive paralysis or locomotion defects as seen in kinesin-1–null larvae. However, late third-instar larvae, which had previously moved vigorously and appeared healthy, abruptly became paralyzed and died. We suspect that this phenotype could be based on a muscle defect, suggesting that MT sliding is also important in nonneuronal tissue. This idea is consistent with a recent study demonstrating the importance of MT sliding and MAP4 regulation during muscle cell differentiation (55).

Interestingly, $Khc^{mutA}$/+ flies, which contain one wild-type copy and one mutant copy of KHC, display intermediate phenotypes: Flies have reduced viability, shorter axons in cultured neurons, and significantly reduced MT sliding. Because kinesin-1 molecules contain two heavy chains, many kinesin-1 molecules in $Khc^{mutA}$/+ flies are likely wild-type KHC and $KHC^{mutA}$ heterodimers, with one wild-type and one deficient MT-binding site. Therefore, the defects observed in $Khc^{mutA}$/+ flies suggest that KHC and $KHC^{mutA}$ heterodimers cannot slide MTs as efficiently as wild-type KHC, and that the C-terminal MT-binding sites on both heavy chains are required for MT sliding. Because MT binding by kinesin-1 is electrostatic, a reduced number of binding sites should lower the binding affinity and could add an additional layer of regulation to MT sliding in the cell. One caveat for these experiments, however, is that the mothers of $Khc^{mutA}$/+ flies were either homozygous or heterozygous $Khc^{mutA}$. It is possible that early developmental defects caused by maternal $Khc^{mutA}$ could be responsible for some of the observed phenotypes instead of a dominant-negative effect.

Previously, we have reported kinesin-1–based MT sliding in tissue culture cells and culture neurons (6, 7, 9). Here, we demonstrate that robust MT sliding occurs in neurons in vivo. This sliding is kinesin-1–dependent and shares the same mechanism as sliding in S2 cells and cultured neurons. Additionally, we have reported that kinesin-1 is required for neurite outgrowth and axon regeneration in cultured neurons (7, 8). Here, we directly test the hypothesis that MT sliding by kinesin-1 drives axon outgrowth. $Khc^{mutA}$ neurons displayed significantly shorter axons in culture and in vivo, suggesting that MT sliding drives axon outgrowth. Expression of an engineered chimeric motor, which can slide MTs but cannot support organelle transport, in $Khc^{mutA}$ neurons rescued axon outgrowth defects in culture and in vivo. These provocative results demonstrate that MT sliding by kinesin-1 is essential for axon outgrowth.

In this study, we have attempted to separate the roles of kinesin-1 in cargo transport and MT–MT sliding. Mutation of kinesin-1's C-terminal MT-binding site ($KHC^{mutA}$) resulted in significantly reduced MT sliding in *Drosophila* S2 cells, primary cultured neurons, and sensory neurons in intact pupae. We have demonstrated that $KHC^{mutA}$ displayed normal affinity for the primary cargo adapter, KLC, as well as for the mitochondrial adapter, Milton. $KHC^{mutA}$ maintains normal peroxisome and mitochondria transport in both *Drosophila* S2 cells and primary cultured neurons. No defects in SYT transport were detected in segmental nerves in vivo, and Rab5 vesicle distribution and transport were maintained in class IV da neurons in $Khc^{mutA}$ larvae. However, mild accumulation of CSP was observed in the segmental nerves of $Khc^{mutA}$ animals, raising the possibility that defects in CSP transport might contribute to some $Khc^{mutA}$ phenotypes. However, we also observed mild accumulation of CSP in other genotypes [$Khc^{27}$/+ and *Df(Unc-76)*/+], which did not result in locomotion and viability defects. However, we cannot rule out the possibility that CSP accumulation in segmental nerves may contribute to some $Khc^{mutA}$ phenotypes.

Finally, we demonstrate a previously unidentified role of MT sliding in dendritic outgrowth in da sensory neurons. $Khc^{mutA}$ larvae display reduced dendritic branching and total dendrite length in class I and IV da neurons, suggesting that MT sliding is important for arborization. This result is consistent with a previous study in *C. elegans*, where the authors demonstrate that mutations in the C terminus of the kinesin-1 ortholog, *unc-116*, result in dendritic phenotypes in vivo (11). A *unc-116* truncation mutant lacking the C terminus, including the MT-binding site, displayed axon-like MT polarity in dendrites, as well as mislocalization of axonal cargoes to dendrites. Additionally, the authors observe the same phenotype using a mutation of the C-terminal MT-binding site analogous to the $KHC^{mutA}$ mutation. Consistent with our data, their MT-binding site mutant also rescues mitochondria transport. The authors speculate that kinesin-1/*unc-116* transports MTs to organize dendritic MT arrays.

Because of the high conservation of the C-terminal MT-binding site of kinesin-1 and important nervous system phenotypes observed in both *Drosophila* and *C. elegans*, we speculate that MT sliding plays an important physiological role in all organisms. Consistent with this idea, we have observed MT sliding in vertebrate cells (6). Furthermore, we demonstrated that human kinesin-1, KIF5B, can slide MTs and generate cellular projections in *Drosophila* S2 cells depleted of endogenous kinesin-1, suggesting KIF5B also engages in sliding. Future studies of kinesin-1–driven MT sliding are warranted in mammalian systems and may provide new insight into the early formation and pathology of the human nervous system.

## Materials and Methods

Additional information is available in the detailed *SI Materials and Methods*.

**MT Sliding Analysis.** A custom Java-based Fiji plug-in was developed to quantify MT sliding rates using the following methodology. Time-lapse movies of photoconverted microtubules were bleach-corrected and thresholded to detect MTs. The initial photoconverted zone was identified, and the number of pixels corresponding to MTs was measured in total or outside the initial zone for each frame. The motile fraction of MTs was calculated for each frame by the following equation: $\%MF = MTs^{outside\_initial\_zone}/MTs^{total}$. These values were then plotted against time, and the slope of this graph was calculated for the initial linear section (identified by the highest $R^2$ value of a linear regression containing at least four data points). This slope represents the gross MT sliding rate in each cell with the units: Change in % Motile Fraction * $min^{-1}$.

To measure MT sliding in bristle neurons in vivo, a Fiji plug-in, StackReg (>Translation), was used to align the position of the neurons, reducing the effect of small movements of the animal during imaging. Then, another Fiji plug-in, Bleach Correction (>Histogram), was used to minimize the bleaching effect of the red signal. Finally, the fluorescence intensity outside the initial photoconverted zone was measured at 0 min and 20 min. The percentage of fluorescence leaving the converted zone was used to indicate the level of MT sliding in these neurons, which was determined by the following equation: $(Fluorescence^{outside\_20min} - Fluorescence^{outside\_0min})/Fluorescence^{total\_20min}$.

**Organelle Transport Analysis.** Peroxisome transport and mitochondria transport were quantified by the particle-tracking software DiaTrack 3.04 (56). To determine average run length, all active transport events (particle run lengths) were defined as having a span of >0.5 μm and lifetime of longer

than four frames. All run lengths in each time-lapse movie were summed and divided by total number of particles (both motile and immotile), resulting in the average run length per cell. To determine the distribution of run lengths, run lengths in each cell were binned with a bin width of 1 μm using Prism 6 (GraphPad) and divided by the total particle count, resulting in the fraction of run lengths in each bin. To determine average particle velocities, particles were tracked for at least four frames and their velocity was calculated; the average velocity of all particles was then determined per cell (including slow and immotile particles). To determine the distribution of particle velocities, individual velocities were binned with a bin width of 50 nm·s$^{-1}$ on Prism 6 and divided by the total count, resulting in the fraction of velocities in each bin.

**ACKNOWLEDGMENTS.** We thank Dr. Chris Q. Doe (University of Oregon), Dr. Melissa Rolls (Penn State University), Dr. William M. Saxton (University of California, Santa Cruz), and the Bloomington Stock Center (NIH P40OD018537) for fly stocks. The mouse monoclonal anti-Futsch (22C10) antibody contributed by Seymour Benzer (California Institute of Technology), CSP (DCSP-2, 6D6) monoclonal antibody contributed by Seymour Benzer, and SYT (3H2 2D7) monoclonal antibody contributed by Kai Zinn (California Institute of Technology) were obtained from the Developmental Studies Hybridoma Bank, created by the NICHD of the NIH and maintained at the Department of Biology, University of Iowa. We also thank the Center for Advanced Microscopy at Northwestern University and Constadina Arvanitis for assistance in imaging YFP-Rab5 vesicles in class IV da neurons. The research reported here was supported by the National Institute of General Medical Science of the NIH under Award R01GM052111 (to V.I.G.).

1. Zhang XF, Hyland C, Van Goor D, Forscher P (2012) Calcineurin-dependent cofilin activation and increased retrograde actin flow drive 5-HT-dependent neurite outgrowth in Aplysia bag cell neurons. *Mol Biol Cell* 23(24):4833–4848.
2. Dent EW, Gupton SL, Gertler FB (2011) The growth cone cytoskeleton in axon outgrowth and guidance. *Cold Spring Harb Perspect Biol* 3(3):a001800.
3. Flynn KC, et al. (2012) ADF/cofilin-mediated actin retrograde flow directs neurite formation in the developing brain. *Neuron* 76(6):1091–1107.
4. Bradke F, Dotti CG (1999) The role of local actin instability in axon formation. *Science* 283(5409):1931–1934.
5. Marsh L, Letourneau PC (1984) Growth of neurites without filopodial or lamellipodial activity in the presence of cytochalasin B. *J Cell Biol* 99(6):2041–2047.
6. Jolly AL, et al. (2010) Kinesin-1 heavy chain mediates microtubule sliding to drive changes in cell shape. *Proc Natl Acad Sci USA* 107(27):12151–12156.
7. Lu W, Fox P, Lakonishok M, Davidson MW, Gelfand VI (2013) Initial neurite outgrowth in Drosophila neurons is driven by kinesin-powered microtubule sliding. *Curr Biol* 23(11):1018–1023.
8. Lu W, Lakonishok M, Gelfand VI (2015) Kinesin-1-powered microtubule sliding initiates axonal regeneration in Drosophila cultured neurons. *Mol Biol Cell* 26(7): 1296–1307.
9. del Castillo U, Lu W, Winding M, Lakonishok M, Gelfand VI (2015) Pavarotti/MKLP1 regulates microtubule sliding and neurite outgrowth in Drosophila neurons. *Curr Biol* 25(2):200–205.
10. Roossien DH, Lamoureux P, Miller KE (2014) Cytoplasmic dynein pushes the cytoskeletal meshwork forward during axonal elongation. *J Cell Sci* 127(Pt 16):3593–3602.
11. Yan J, et al. (2013) Kinesin-1 regulates dendrite microtubule polarity in Caenorhabditis elegans. *eLife* 2:e00133.
12. Roossien DH, Lamoureux P, Van Vactor D, Miller KE (2013) Drosophila growth cones advance by forward translocation of the neuronal cytoskeletal meshwork in vivo. *PLoS One* 8(11):e80136.
13. Saxton WM, Hicks J, Goldstein LS, Raff EC (1991) Kinesin heavy chain is essential for viability and neuromuscular functions in Drosophila, but mutants show no defects in mitosis. *Cell* 64(6):1093–1102.
14. Brendza KM, Rose DJ, Gilbert SP, Saxton WM (1999) Lethal kinesin mutations reveal amino acids important for ATPase activation and structural coupling. *J Biol Chem* 274(44):31506–31514.
15. Navone F, et al. (1992) Cloning and expression of a human kinesin heavy chain gene: interaction of the COOH-terminal domain with cytoplasmic microtubules in transfected CV-1 cells. *J Cell Biol* 117(6):1263–1275.
16. Hackney DD, Stock MF (2000) Kinesin's IAK tail domain inhibits initial microtubule-stimulated ADP release. *Nat Cell Biol* 2(5):257–260.
17. Seeger MA, Rice SE (2010) Microtubule-associated protein-like binding of the kinesin-1 tail to microtubules. *J Biol Chem* 285(11):8155–8162.
18. Wong YL, Rice SE (2010) Kinesin's light chains inhibit the head- and microtubule-binding activity of its tail. *Proc Natl Acad Sci USA* 107(26):11781–11786.
19. Barlan K, Lu W, Gelfand VI (2013) The microtubule-binding protein ensconsin is an essential cofactor of kinesin-1. *Curr Biol* 23(4):317–322.
20. McKinney SA, Murphy CS, Hazelwood KL, Davidson MW, Looger LL (2009) A bright and photostable photoconvertible fluorescent protein. *Nat Methods* 6(2):131–133.
21. Subach OM, Cranfill PJ, Davidson MW, Verkhusha VV (2011) An enhanced monomeric blue fluorescent protein with the high chemical stability of the chromophore. *PLoS One* 6(12):e28674.
22. Kural C, et al. (2005) Kinesin and dynein move a peroxisome in vivo: A tug-of-war or coordinated movement? *Science* 308(5727):1469–1472.
23. Tomishige M, Klopfenstein DR, Vale RD (2002) Conversion of Unc104/KIF1A kinesin into a processive motor after dimerization. *Science* 297(5590):2263–2267.
24. Kuznetsov SA, et al. (1988) The quaternary structure of bovine brain kinesin. *EMBO J* 7(2):353–356.
25. Glater EE, Megeath LJ, Stowers RS, Schwarz TL (2006) Axonal transport of mitochondria requires milton to recruit kinesin heavy chain and is light chain independent. *J Cell Biol* 173(4):545–557.
26. Ling SC, Fahrner PS, Greenough WT, Gelfand VI (2004) Transport of Drosophila fragile X mental retardation protein-containing ribonucleoprotein granules by kinesin-1 and cytoplasmic dynein. *Proc Natl Acad Sci USA* 101(50):17428–17433.
27. Gould SJ, Keller GA, Hosken N, Wilkinson J, Subramani S (1989) A conserved tripeptide sorts proteins to peroxisomes. *J Cell Biol* 108(5):1657–1664.
28. Hurd DD, Saxton WM (1996) Kinesin mutations cause motor neuron disease phenotypes by disrupting fast axonal transport in Drosophila. *Genetics* 144(3):1075–1085.
29. Huang J, Zhou W, Dong W, Watson AM, Hong Y (2009) From the Cover: Directed, efficient, and versatile modifications of the Drosophila genome by genomic engineering. *Proc Natl Acad Sci USA* 106(20):8284–8289.
30. Groth AC, Fish M, Nusse R, Calos MP (2004) Construction of transgenic Drosophila by using the site-specific integrase from phage phiC31. *Genetics* 166(4):1775–1782.
31. Huang J, Zhou W, Watson AM, Jan YN, Hong Y (2008) Efficient ends-out gene targeting in Drosophila. *Genetics* 180(1):703–707.
32. Nichols CD, Becnel J, Pandey UB (2012) Methods to assay Drosophila behavior. *J Vis Exp* (61):3795.
33. Campos AR, Rosen DR, Robinow SN, White K (1987) Molecular analysis of the locus elav in Drosophila melanogaster: A gene whose embryonic expression is neural specific. *EMBO J* 6(2):425–431.
34. Robinow S, White K (1988) The locus elav of Drosophila melanogaster is expressed in neurons at all developmental stages. *Dev Biol* 126(2):294–303.
35. Lu W, et al. (2016) Microtubule–microtubule sliding by kinesin-1 is essential for normal cytoplasmic streaming in *Drosophila* oocytes. *Proc Natl Acad Sci USA* 113: E4995–E5004.
36. del Castillo U, Winding M, Lu W, Gelfand VI (2015) Interplay between kinesin-1 and cortical dynein during axonal outgrowth and microtubule organization in Drosophila neurons. *eLife* 4:e10140.
37. Karle KN, Möckel D, Reid E, Schöls L (2012) Axonal transport deficit in a KIF5A( -/- ) mouse model. *Neurogenetics* 13(2):169–179.
38. Ferreira A, Niclas J, Vale RD, Banker G, Kosik KS (1992) Suppression of kinesin expression in cultured hippocampal neurons using antisense oligonucleotides. *J Cell Biol* 117(3):595–606.
39. Rhyu MS, Jan LY, Jan YN (1994) Asymmetric distribution of numb protein during division of the sensory organ precursor cell confers distinct fates to daughter cells. *Cell* 76(3):477–491.
40. Simpson P, Woehl R, Usui K (1999) The development and evolution of bristle patterns in Diptera. *Development* 126(7):1349–1364.
41. Hadjieconomou D, Timofeev K, Salecker I (2011) A step-by-step guide to visual circuit assembly in Drosophila. *Curr Opin Neurobiol* 21(1):76–84.
42. Martin M, et al. (1999) Cytoplasmic dynein, the dynactin complex, and kinesin are interdependent and essential for fast axonal transport. *Mol Biol Cell* 10(11):3717–3728.
43. Gindhart JG, et al. (2003) The kinesin-associated protein UNC-76 is required for axonal transport in the Drosophila nervous system. *Mol Biol Cell* 14(8):3356–3365.
44. Blasius TL, Cai D, Jih GT, Toret CP, Verhey KJ (2007) Two binding partners cooperate to activate the molecular motor Kinesin-1. *J Cell Biol* 176(1):11–17.
45. Satoh D, et al. (2008) Spatial control of branching within dendritic arbors by dynein-dependent transport of Rab5-endosomes. *Nat Cell Biol* 10(10):1164–1171.
46. Sholl DA (1953) Dendritic organization in the neurons of the visual and motor cortices of the cat. *J Anat* 87(4):387–406.
47. Hwang RY, Stearns NA, Tracey WD (2012) The ankyrin repeat domain of the TRPA protein painless is important for thermal nociception but not mechanical nociception. *PLoS One* 7(1):e30090.
48. Mauthner SE, et al. (2014) Balboa binds to pickpocket in vivo and is required for mechanical nociception in Drosophila larvae. *Curr Biol* 24(24):2920–2925.
49. Zhong L, Hwang RY, Tracey WD (2010) Pickpocket is a DEG/ENaC protein required for mechanical nociception in Drosophila larvae. *Curr Biol* 20(5):429–434.
50. Robertson JL, Tsubouchi A, Tracey WD (2013) Larval defense against attack from parasitoid wasps requires nociceptive neurons. *PLoS One* 8(10):e78704.
51. Hwang RY, et al. (2007) Nociceptive neurons protect Drosophila larvae from parasitoid wasps. *Curr Biol* 17(24):2105–2116.
52. Tanaka Y, et al. (1998) Targeted disruption of mouse conventional kinesin heavy chain, kif5B, results in abnormal perinuclear clustering of mitochondria. *Cell* 93(7): 1147–1158.
53. Pilling AD, Horiuchi D, Lively CM, Saxton WM (2006) Kinesin-1 and Dynein are the primary motors for fast transport of mitochondria in Drosophila motor axons. *Mol Biol Cell* 17(4):2057–2068.
54. Gindhart JG, Jr, Desai CJ, Beushausen S, Zinn K, Goldstein LS (1998) Kinesin light chains are essential for axonal transport in Drosophila. *J Cell Biol* 141(2):443–454.
55. Mogessie B, Roth D, Rahil Z, Straube A (2015) A novel isoform of MAP4 organises the paraxial microtubule array required for muscle cell differentiation. *eLife* 4:e05697.
56. Vallotton P, Olivier S (2013) Tri-track: Free software for large-scale particle tracking. *Microsc Microanal* 19(2):451–460.
57. Halachmi N, Nachman A, Salzberg A (2012) Visualization of proprioceptors in *Drosophila* larvae and pupae. *J Vis Exp* (64):3846.